J|A|C|S
ARTICLES
Published on Web 04/07/2005

Pyrolysis of Mesoporous Silica-Immobilized 1,3-Diphenylpropane. Impact of Pore Confinement and Size

Michelle K. Kidder,[†] Phillip F. Britt,[†] Zongtao Zhang,[†] Sheng Dai,[†] Edward W. Hagaman,[†] Alan L. Chaffee,[‡] and A. C. Buchanan, III*,[†]

Contribution from the Chemical Sciences Division, Oak Ridge National Laboratory, Oak Ridge, Tennessee 37831-6197, and School of Chemistry, Monash University, Victoria, Australia

Received January 20, 2005; E-mail: buchananac@ornl.gov

Abstract: Mesoporous silicas such as SBA-15 and MCM-41 are being actively investigated for potential applications in catalysis, separations, and synthesis of nanostructured materials. A new method for functionalizing these mesoporous silicas with aromatic phenols is described. The resulting novel hybrid materials possess silyl aryl ether linkages to the silica surface that are thermally stable to ca. 550 °C, but can be easily cleaved at room temperature with aqueous base for quantitative recovery of the organic moieties. The materials have been characterized by nitrogen physisorption, FTIR, NMR, and quantitative analysis of surface coverages. The maximum densities of 1,3-diphenylpropane (DPP) molecules that could be grafted to the surface were less than those measured on a nonporous, fumed silica (Cabosil) and were also found to decrease as a function of decreasing pore size (5.6−1.7 nm). This is a consequence of steric congestion in the pores that is magnified at the smaller pore sizes, consistent with parallel studies conducted using a conventional silylating reagent, 1,1,3,3-tetramethyldisilazane. Pyrolysis of the silica-immobilized DPP revealed that pore confinement leads to enhanced rates and altered product selectivity for this free-radical reaction compared with the nonporous silica, and the rates and selectivities also depended on pore size. The influence of confinement is discussed in terms of enhanced encounter frequencies for bimolecular reaction steps and pore surface curvature that alters the accessibility and resultant selectivity for hydrogen transfer steps.

Introduction

Ordered mesoporous silicas continue to be widely investigated because of their many potential applications in catalysis,[1] separations,[2] and the synthesis of novel nanostructured materials.[3] These silicas are appealing because of their high surface area, ordered pore structure of varying morphologies, and control of pore size over wide ranges.[4] Furthermore, organic−inorganic hybrid materials are readily prepared and used to introduce organic functional groups or to modify the surface properties.[4b,5] The organic functionality can be introduced by co-condensation during the template-directed synthesis of the mesoporous materials or by post-synthetic grafting strategies utilizing the silanol groups in the mesoporous silicas. An advantage of the grafting technique is that the original ordered pore structure is easily maintained, although the size and number of the groups that can be introduced may be limited by the size of the pores.[5c] Currently, functionalization typically involves the reaction of the surface silanol groups (≡Si−OH) with silane coupling agents such as silyl chlorides (R_3Si-Cl), silyl alkoxides (R_3Si-OR), and disilazanes ($R_3Si-NH-SiR_3$), which result in siloxane linkages (≡Si− O−SiR_3) to the surface.[5a,6] In a recent communication, we briefly reported a new method for functionalizing mesoporous silicas utilizing a phenol functional group as the coupling agent, as shown in Figure 1.[7] This condensation reaction establishes a silyl ether linkage (≡Si−O−C_{aryl}) to the surface. This linkage is thermally stable to ca. 550 °C, which

[†] Oak Ridge National Laboratory.
[‡] Monash University.

(1) (a) Thomas, J. M.; Johnson, B. F. G.; Raja, R.; Sankar, G.; Midgely, P. A. *Acc. Chem. Res.* **2003**, *36*, 20. (b) Brunel, D.; Blanc, A. C.; Galarneau, A.; Fajula, F. *Catal. Today* **2002**, *73*, 139. (c) Dufaud, V.; Davis, M. E. *J. Am. Chem. Soc.* **2003** *125*, 9403. (d) Nozaki, C.; Lugmair, C. G.; Bell, A. T.; Tilley, T. D. *J. Am. Chem. Soc.* **2002**, *124*, 13194. (e) McKittrick, M. W.; Jones, C. W. *J. Am. Chem. Soc.* **2004**, *126*, 3052. (f) Humphrey, H. P. Y.; Wright, P. A.; Botting, N. P. *J. Mol. Catal. B: Enzym.* **2001**, *15*, 81. (g) Iwamoto, M.; Tanaka, Y.; Sawamura, N.; Namba, S. *J. Am. Chem. Soc.* **2003**, *125*, 13032.

(2) (a) Lee, B.; Bao, L.-L.; Im, H.-J.; Dai, S.; Hagaman, E. W.; Lin, J. S. *Langmuir* **2003**, *19*, 4246. (b) Ueno, Y.; Tate, A.; Niwa, O.; Zhou, H.-S.; Yamada, T.; Honma, I. *Chem. Commun.* **2004**, 746. (c) Lin, Y.; Fryxell, G. E.; Wu, H.; Engelhard, M. *Environ. Sci. Technol.* **2001**, *35*, 3962. (d) Yoshitake, H.; Yokoi, T.; Tatsumi, T. *Chem. Mater.* **2002**, *14*, 4603. (e) Newalkar, B. L.; Choudary, N. V.; Kumar, P.; Kormarneni, S.; Bhat, T. S. G. *Chem. Mater.* **2002**, *14*, 304. (f) Ding, J. D.; Hudalla, C. J.; Cook, J. T.; Walsh, D. P.; Boissel, C. E.; Iraneta, P. C.; O'Gara, J. E. *Chem. Mater.* **2004**, *16*, 670.

(3) (a) Che, S.; Liu, Z.; Ohsuna, T.; Sakamoto, K.; Terasaki, O.; Tatsumi, T. *Nature* **2004**, *429*, 281. (b) Inagaki, S.; Guan, S.; Ohsuno, T.; Terasaki, O. *Nature* **2002**, *416*, 304. (c) Stein, A.; Melde, B. J.; Schroden, R. C. *Adv. Mater.* **2000**, *19*, 1403. (d) Li, Z.; Jaroniec, M. *J. Am. Chem. Soc.* **2001**, *123*, 9208. (e) Asefa, T.; Kruk, M.; Coombs, N.; Grondey, H.; MacLachlan, M. J.; Jaroniec, M.; Ozin, G. A. *J. Am. Chem. Soc.* **2003**, *125*, 11662.

(4) (a) Lin, H.-P.; Mou, C.-Y. *Acc. Chem. Res.* **2002**, *35*, 927. (b) Anwander, R. *Chem. Mater.* **2001**, *13*, 4419.

(5) (a) Stein, A.; Melde, B. J.; Schroden, R. C. *Adv. Mater.* **2000**, *19*, 1403. (b) Huh, S.; Wiench, J. W.; Trewyn, B. G.; Song, S.; Pruski, M.; Lin, V. S.-Y. *Chem. Commun.* **2003**, 2364. (c) Antochshuk, V.; Kruk, M.; Jaroniec, M. *J. Phys. Chem. B* **2003**, *107*, 11900.

(6) (a) Anwander, R.; Nagl, I.; Widenmeyer, M.; Engelhardt, G.; Groeger, O.; Palm, C.; Roser, T. *J. Phys. Chem. B* **2000**, *104*, 3532. (b) Widenmeyer, M.; Anwander, R. *Chem. Mater.* **2002**, *14*, 1827.

(7) Kidder, M. K.; Britt, P. F.; Zhang, Z.; Dai, S.; Buchanan, A. C., III. *Chem. Commun.* **2003**, 2804.

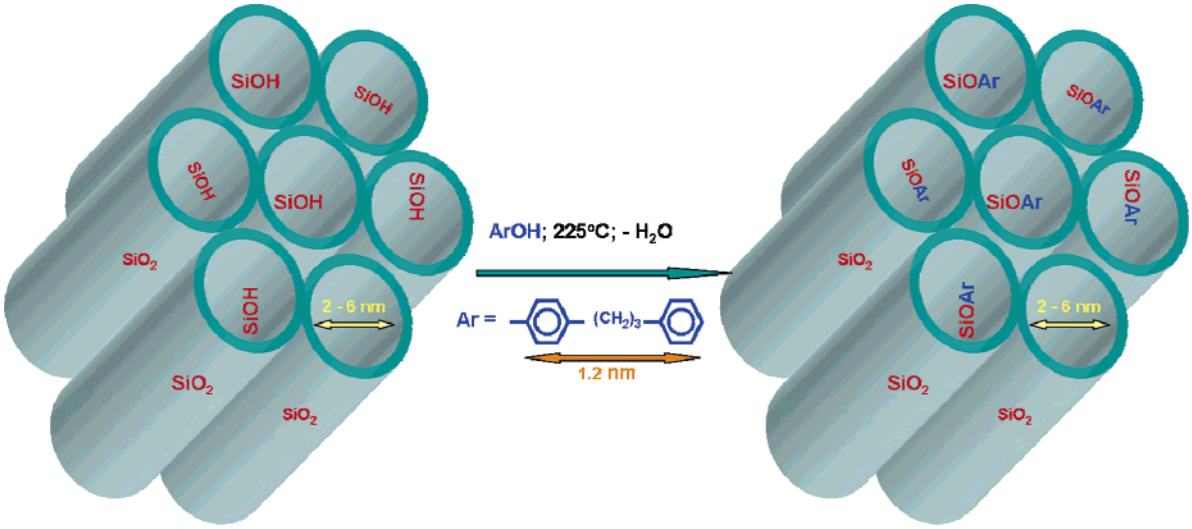

Figure 1. Phenol coupling with silanols for synthesis of organically modified hexagonal mesoporous silicas with tunable pore sizes.

permits the study of chemical reactions on the surface at high temperatures. In addition, the linkage can be cleaved at room temperature with aqueous base so that surface-bound products are easily retrieved for analysis. In this article, we provide a full account of the synthesis and characterization of these novel hybrid materials.

We have also been interested in exploring the impacts of surface immobilization on high-temperature, organic free-radical reactions to understand the impacts of restricted mass transport on reaction kinetics and mechanisms, and our previous studies have utilized nonporous fumed silica nanoparticles (Cabosil) as the support.[8] Organic radical chemistry on surfaces continues to draw considerable attention[9] with a recent focus on the synthesis of nanostructured materials.[10] In this article, we describe research on the effects of pore confinement on a free-radical reaction through comparison of the Cabosil and mesoporous silica supports. Since the pore size of the mesoporous silicas can be systematically varied (5.6−1.7 nm in the current study), the influence of pore radius-of-curvature can be examined. Although pore size and shape play an important role in controlling chemical reactivity in zeolites,[9a,b,g] there is much less known about pore size effects in mesoporous materials. This study will address this important fundamental issue. Interestingly, changes in pore size have been recently linked to changes in activity of catalytic sites in mesoporous catalysts,[1g,11] for example, vanadium oxidation catalysts supported on MCM-41 silicas.[11]

Pyrolysis of surface-immobilized 1,3-diphenylpropane (DPP) is being used as a convenient free-radical probe reaction to examine the impacts of pore confinement. We have examined this reaction in detail on the nonporous Cabosil silica surface.[12] As shown in Scheme 1, pyrolysis at 375 °C produces a simple mixture of products, gas-phase and surface-attached toluene and styrene, in comparable amounts. The underlying free-radical decay pathway is an efficient chain process with kinetic chain lengths exceeding 250. The propagation steps involve gas-phase and surface-attached benzyl radicals abstracting hydrogen from DPP to form the toluene products (Scheme 1). Fast unimolecular β-scission of the resulting regiochemically distinct radicals, **1** and **2**, forms the styrene products while regenerating the two benzyl radicals. The overall rate of DPP pyrolysis is controlled by the rates of the bimolecular hydrogen transfer steps, while the product selectivity is determined by the relative rates of formation of **1** and **2**. In this article, we show that pore confinement leads to alterations in both the reaction rate and product selectivity.

Experimental Section

Characterization. BET specific surface areas were obtained from nitrogen adsorption−desorption isotherms measured at 77 K on a Quantochrome Autosorb-1 analyzer with all samples outgassed at 100 °C for 6 h prior to analysis. Native mesoporous silicas were also dried at 200 °C for 4 h before outgassing. Micropore surface areas for SBA-15 samples were determined by the t-method. Pore size distributions were analyzed by the BJH method. Infrared spectra were recorded in the diffuse reflectance mode on a BioRad FTS 3000MX FTIR spectrometer. NMR measurements were recorded on a Varian (CMX

(8) (a) Buchanan, A. C., III; Kidder, M. K.; Britt, P. F. *J. Am. Chem. Soc.* **2003**, *125*, 11806. (b) Buchanan, A. C., III; Britt, P. F.; Thomas, K. B.; Biggs, C. A. *J. Am. Chem. Soc.* **1996**, *118*, 2182. (c) Buchanan, A. C., III; Britt, P. F. *J. Anal. Appl. Pyrolysis* **2000**, *54*, 127. (d) Britt, P. F.; Buchanan, A. C., III; Malcolm, E. A. *Energy Fuels* **2000**, *14*, 1314. (e) Buchanan, A. C., III; Britt, P. F.; Skeen, J. T.; Struss, J. A.; Elam, C. L. *J. Org. Chem.* **1998**, *63*, 9895. (f) Buchanan, A. C., III; Britt, P. F.; Koran, L. J. *Energy Fuels* **2002**, *16*, 517. (g) Buchanan, A. C., III; Britt, P. F.; Thomas, K. B. *Energy Fuels* **1998**, *12*, 649. (h) Buchanan, A. C., III; Kidder, M. K.; Britt, P. F. *J. Phys. Chem. B* **2004**, *108*, 16772.

(9) (a) Turro, N. J. *Chem. Commun.* **2002**, 2279. (b) Rouhi, A. M. *Chem. Eng. News* **2000**, *78* (Aug 21), 40. (c) Nagl, I.; Widenmeyer, M.; Grasser, S.; Kohler, K.; Anwander, R. *J. Am. Chem. Soc.* **2000**, *122*, 1544. (d) Turro, N. J.; Lei, X.-G.; Jockusch, S.; Li, W.; Liu, Z.; Abrams, L.; Ottaviani, M. F. *J. Org. Chem.* **2002**, *67*, 2606. (e) Lee, C.-H.; Lim, T.-S.; Mou, C. Y. *Phys. Chem. Chem. Phys.* **2002**, *4*, 3106. (f) Kretzschmar, I.; Friend, C. M.; Sigman, M. E. *J. Phys. Chem. B* **2002**, *106*, 663. (g) Gu, W.; Warrier, M.; Ramamurthy, V.; Weiss, R. G. *J. Am. Chem. Soc.* **1999**, *121*, 9467. (h) Chen, Y.; Kervio, E.; Rétey, J. *Helv. Chim. Acta* **2002**, *85*, 552.

(10) (a) Wang, J.-Y.; Chen, W.; Liu, A.-H.; Lu, G.; Zhang, G.; Zhang, J.-H.; Yang, B. *J. Am. Chem. Soc.* **2002**, *124*, 13358. (b) Blomberg, S.; Ostberg, S.; Harth, E.; Bosman, A. W.; van Horn, B.; Hawker, C. J. *J. Polym. Sci., Part A: Polym. Chem.* **2002**, *40*, 1309. (c) Carrot, G.; Diamanti, S.; Manuszak, M.; Charleux, B.; Vairon, J. P. *J. Polym. Sci., Part A: Polym. Chem.* **2001**, *39*, 4294. (d) Xiao, D.; Wirth, M. J. *Macromolecules* **2002**, *35*, 2919. (e) Lopinski, G. P.; Wayner, D. D. M.; Wolkow, R. A. *Nature* **2000**, *406*, 48. (f) Tong, X.; DiLabio, G. A.; Clarkin, O. J.; Wolkow, R. A. *Nano Lett.* **2004**, *4*, 357. (g) Tong, X.; DiLabio, G. A.; Wolkow, R. A. *Nano. Lett.* **2004**, *4*, 979. (h) Tsujii, Y.; Ejaz, M.; Sato, K.; Goto, A.; Fukuda, T. *Macromolecules* **2001**, *34*, 8872. (i) Tomlinson, M. R.; Genzer, J. *Chem. Commun.* **2003**, 1350. (j) Huseman, M.; Morrison, M.; Benoit, D.; Frommer, J.; Mate, C. M.; Hinsberg, W. D.; Hedrick, J. L.; Hawker, C. J. *Langmuir* **2000**, *122*, 1844. (k) Granville, A. M.; Boyes, S. G.; Akgun, B.; Foster, M. D.; Brittain, W. J. *Macromolecules* **2004**, *37*, 2790.

(11) Haller, G. L. *J. Catal.* **2003**, *216*, 12 and references therein.

(12) Buchanan, A. C., III; Biggs, C. A. *J. Org. Chem.* **1989**, *54*, 517.

Scheme 1. Products from Pyrolysis of Silica-Immobilized 1,3-Diphenylpropane and Propagation Steps for the Radical Chain Decomposition Mechanism

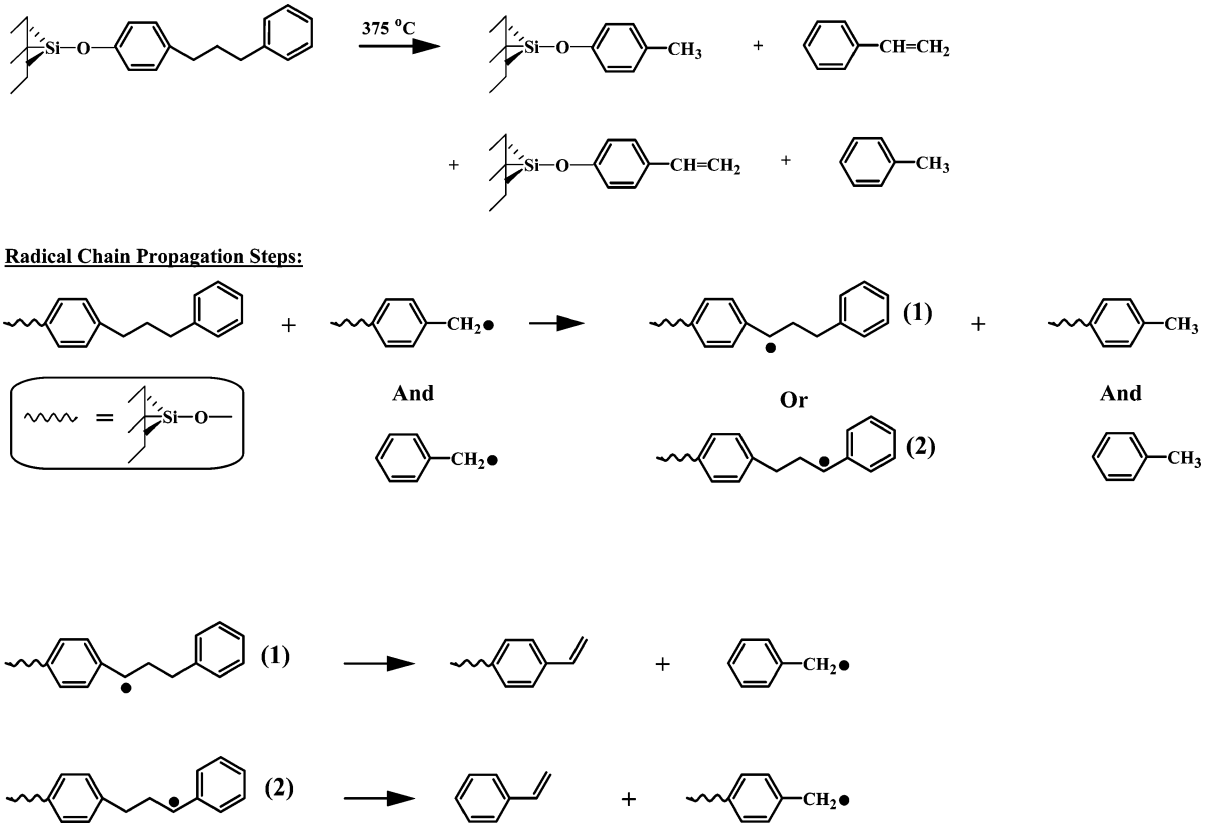

Infinity) spectrometer operating at 2.42 T. ^{13}C NMR spectra were obtained at 25.89 MHz using standard $^{1}H-^{13}C$ CP/MAS techniques.[13] The magic angle spinning speed was 4.5 kHz. The ^{1}H 90° pulse width was set to 3.1 μs ($H_{1H} = 81$ kHz), and the Hartmann−Hahn CP match condition was satisfied at the first upper sideband. The normal recycle delay of 1 s was increased to 3 s for relaxation measurements. Chemical shifts were referenced externally to the methyl resonance of hexamethylbenzene (17.3 ppm relative to TMS at 0 ppm). ^{13}C T_1 measurements were performed using the CP version of the Freeman−Hill T_1 experiment.[14] GC analyses were performed on a Hewlett-Packard 5890 series II gas chromatograph employing a J & W Scientific 30 m × 0.25 mm DB-5 MS column (0.25 μM film thickness) and flame ionization detection. Detector response factors were determined relative to cumene (hydrocarbon products) or 2,5-dimethylphenol and *p*-hydroxybiphenyl (phenolic products) as internal standards. Mass spectra were obtained at 70 eV with a Hewlett-Packard 5972A/5890 series II GC−MS equipped with a capillary column matched to that used for GC analyses. Carbon elemental analyses of organically modified silicas were determined by Galbraith Laboratories, Knoxville, TN.

Materials. SBA-15 amd MCM-41 hexagonal mesoporous silicas were synthesized following standard procedures as described by Jarupatrakorn and Tilley.[15] The three MCM-41 samples of 2.9, 2.2, and 1.7 nm average pore diameter were prepared utilizing $C_nH_{2n+1}N(CH_3)_3Br$ (n = 16, 14, 12, respectively) as the structure directing templates. Cabosil M-5 silica (200 m^2/g; 12-nm particle size) was obtained from Cabot Corporation.

Benzene was distilled from sodium immediately prior to use. High purity acetone and dichloromethane were commercially available and used as received. Cumene was fractionally distilled (2×), and 2,5-dimethylphenol was recrystallized from ethanol. Synthesis of *p*-(3-phenylpropyl)phenol (HODPP) has been previously described.[12]

Preparation of Silylated Derivatives. The silicas were silylated with commercially available 1,1,3,3-tetramethyldisilazane according to the procedure of Anwander et al.[6a] In general, the silicas were dried at 200 °C for 4 h and then cooled in a desiccator. Then, the disilazane reagent (5 mmol) in hexane (5 mL) was added to the dry silica (0.1−0.2 g) suspended in hexane (10 mL). The mixture was stirred at room temperature under argon for 24 h, followed by filtration through a fine fritted filter. The solid residue was washed several times with hexane, and the silylated derivative was then dried under vacuum (5×10^{-3} Torr) at room temperature for 5 h and then at 250 °C for 2 h. The coverage of dimethylsilyl groups ($SiH(CH_3)_2$) bound to the silica surface was determined from carbon elemental analysis.

Preparation of Surface-Attached 1,3-Diphenylpropane. A typical surface attachment reaction is described for the MCM-41 silica with a surface area of 1088 $m^2\ g^{-1}$, which was dried at 200 °C for 4 h prior to use. Excess HODPP (2.7 g, 12.7 mmol) was adsorbed onto the surface of the dried MCM-41 (1 g, ca. 4.5 mmol SiOH assuming a maximum of 2.5 SiOH nm^{-2} derivatizable[6]) by solvent evaporation from a benzene slurry. The attachment reaction was performed at 225 °C for 1 h in a fluidized sand bath on a degassed, evacuated ($<10^{-5}$ Torr) sample sealed in a Pyrex glass tube. The sample was transferred to another tube, connected to a dynamic vacuum at 5×10^{-3} Torr, heated in a tube furnace from 225 to 275 °C at a rate of 10 °C/ min, and held at 275 °C for 10 min to remove unattached HODPP. The samples were stored in a desiccator under vacuum. Surface coverage analysis involved base hydrolysis (1 N NaOH, 30 mL) of a ca. 30-mg sample, addition of *p*-phenylphenol in 1 N NaOH as an internal standard, acidification with HCl, extraction with dichloromethane, drying over $MgSO_4$, filtration, and solvent evaporation. The residue was silylated with *N*,*O*-bis-(trimethylsilyl)trifluoroacetamide/pyridine (1:2) and analyzed via GC. Chemical purities of the recovered DPP moieties by GC analysis were >99.5%. Surface coverages were also independently verified by carbon elemental analysis, which gave the same results within ±3%.

(13) Yannoni, C. S. *Acc. Chem. Res.* **1982**, *15*, 201.
(14) Torchia, D. A. *J. Magn. Reson.* **1978**, *30*, 613.
(15) Jarupatrakorn, J.; Tilley, T. D. *J. Am. Chem. Soc.* **2002**, *124*, 8380.

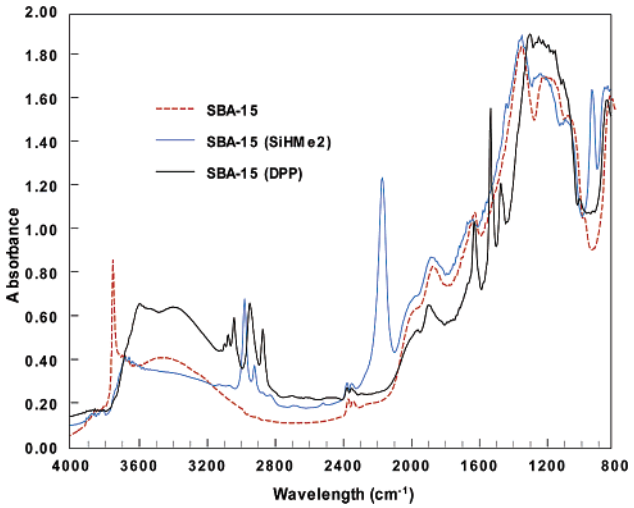

Figure 2. Diffuse reflectance FTIR spectra for SBA-15 and derivatives.

Pyrolysis Procedure. A weighed amount of sample (50−90 mg) was placed in one end of a T-shaped Pyrex tube, evacuated, and sealed at ca. 2×10^{-6} Torr. The sample was inserted into a preheated temperature-controlled, three-zone tube furnace (±1 °C) fitted with a copper sample holder, and the other end was placed in a liquid nitrogen bath. The hydrocarbon products that evolved into the gas phase were collected in the cold trap and dissolved in acetone (0.1−0.2 mL) containing cumene as an internal quantitation standard. These products were analyzed by GC and GC−MS. The surface-attached products were analyzed similarly following base hydrolysis of the solid residue, which liberates the products as phenols, analogous to the surface coverage analysis procedure described above.

Results and Discussion

Nitrogen Physisorption and FTIR Characterization. Large pore SBA-15 and MCM-41 (C-16 template) samples were derivatized with *p*-(3-phenylpropyl)phenol, which introduces 1,3-diphenylpropane (DPP) groups via condensation with the surface silanol groups as illustrated in Figure 1. For comparison, we also prepared silylated derivatives using 1,1,3,3-tetramethyldisilazane, which introduces the dimethylsilyl group (−$SiHMe_2$) and is reported to give the highest silylation efficiency of all the reagents examined.[6a] The FTIR spectra of these derivatives are shown in Figure 2 for the SBA-15 case, and they are consistent with the introduction of the −$SiHMe_2$ (e.g., Si−H stretch at 2152 cm^{-1}; aliphatic C−H stretch at 2970 and 2908 cm^{-1}) and DPP (e.g., aromatic and aliphatic C−H stretch at 3062−2858 cm^{-1}; C═C ring stretch at 1612−1454 cm^{-1}) groups. In each case, the spectra indicate that the isolated silanols (3746 cm^{-1}) have been derivatized. The presence of unreacted, hydrogen-bonded silanols and physisorbed water is also evident, and a quantitative comparison of these derivatization reactions will be presented in the next section.

The nitrogen physisorption isotherms are shown in Figures 3 (SBA-15) and 4 (MCM-41) along with the BJH pore size distributions, and the resulting properties are collected in Table 1.

The isotherms are typical type IV isotherms with the SBA-15 exhibiting a characteristically larger adsorption−desorption hysteresis loop,[16] which is maintained for both the $SiHMe_2$ and DPP derivatives. The details of the origin of this hysteresis behavior is still a problem under active investigation.[16b] From the data in Table 1, it can be seen that the surface area, mean

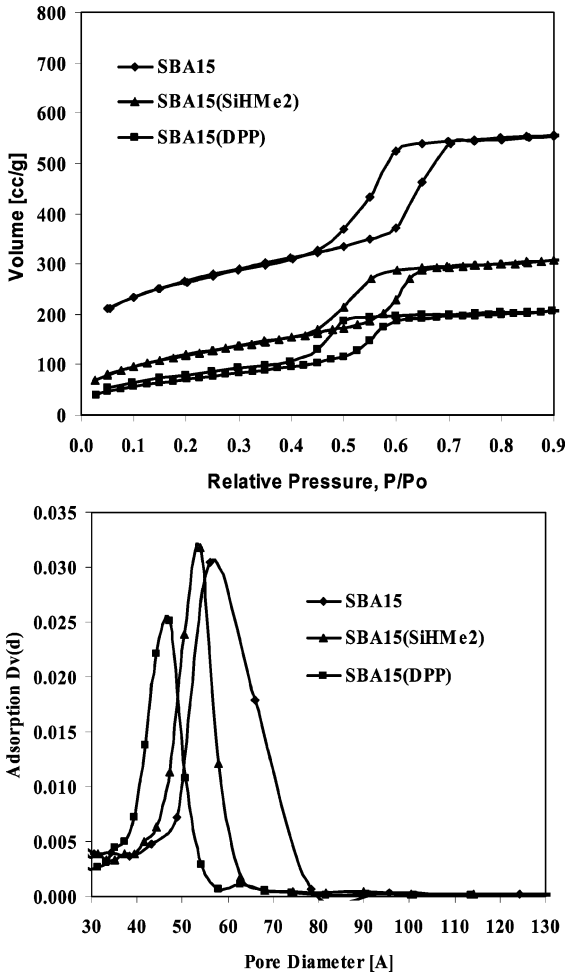

Figure 3. Nitrogen physisorption analysis for SBA-15 samples. Top: adsorption/desorption isotherm. Bottom: BJH pore size distribution.

pore diameter, and pore volume are all smaller for the DPP derivatives compared with the corresponding $SiHMe_2$ derivatives as a consequence of the larger size of the DPP moiety. This is consistent with the results of Anwander et al. who observed similar behavior in MCM-41 samples derivatized with organosilyl groups of varying size.[6a]

In contrast to MCM-41, SBA-15 is known to contain a significant amount of its surface area in micropores, 251 m^2 g^{-1} measured for this sample, that interconnect the mesopores.[6b,16c,17] For both the $SiHMe_2$ and DPP derivatives, no micropore surface area is detected presumably due to pore blocking. Interestingly, the mesopore size distribution is narrower for the two derivatives compared with the native SBA-15. Recent NMR, X-ray diffraction, and modeling studies suggest that the pore surface of SBA-15 is rougher than that of the MCM-41 analogues, presumably related to the presence of the additional micropore structure connecting the mesopores.[16] The narrower pore size distribution for the derivatives could be related to a "surface smoothing effect" that has been proposed for silylated derivatives of large pore, mesitylene-expanded

(16) (a) Shenderovich, I. J.; Buntkowski, G.; Schreiber, A.; Gedat, E.; Sharif, S.; Albrecht, J.; Golubev, N. S.; Findenegg, G. H.; Limbach, H.-H. *J. Phys. Chem. B* **2003**, *107*, 11924. (b) Morishige, K.; Nakamura, Y. *Langmuir* **2004**, *20*, 4503. (c) Imperor-Clerc, M.; Davidson, P.; Davidson, A. *J. Am. Chem. Soc.* **2000**, *122*, 11925.
(17) (a) Joo, S. H.; Ryoo, R.; Kruk, M.; Jaroniec, M. *J. Phys. Chem. B* **2002**, *106*, 4640. (b) Galarneau, A.; Cambon, H.; Di Renzo, F.; Ryoo, R.; Choi, M.; Fajula, F. *New J. Chem.* **2003**, *27*, 73.

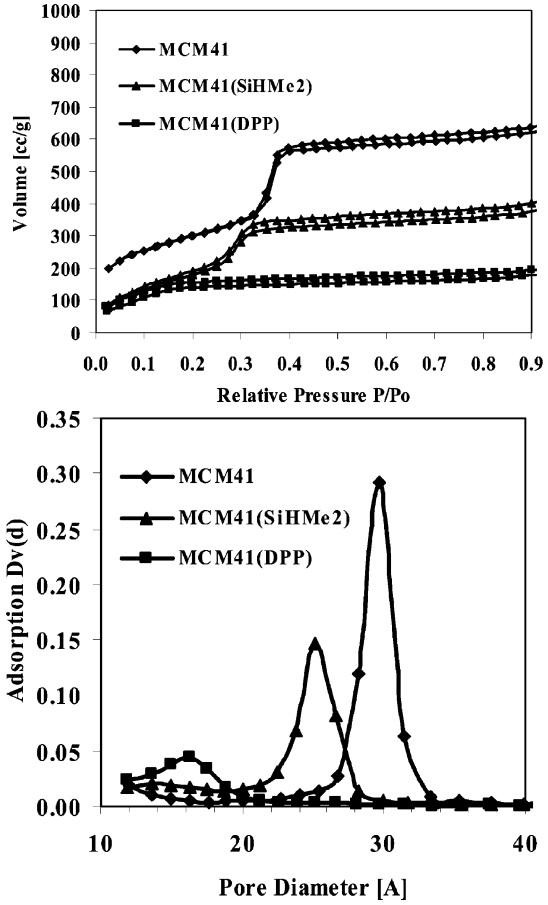

Figure 4. Nitrogen physisorption analysis for MCM-41 samples. Top: adsorption/desorption isotherm. Bottom: BJH pore size distribution.

Table 1. Comparison of Surface Analysis for Organically Modified SBA-15 (5.6 nm) and MCM-41 (2.9 nm)

material[a]	surface area[b] ($m^2\ g^{-1}$)	pore diameter[c] (nm)	pore volume ($cm^3\ g^{-1}$)
SBA-15	867	5.6	0.87
SBA-15 ($SiHMe_2$)	434	5.4	0.49
SBA-15 (DPP)	264	4.7	0.32
MCM-41	1088	2.9	0.99
MCM-41 ($SiHMe_2$)	732	2.5	0.67
MCM-41 (DPP)	619	1.6	0.39

[a] Mesoporous silicas with grafted dimethylsilyl ($SiHMe_2$) and 1,3-diphenylpropane (DPP) groups. [b] BET specific surface area. [c] Mean pore diameter determined by the BJH method on the adsorption branch.

MCM silicas.[6a] The mean pore diameter of the DPP derivatives of SBA-15 and MCM-41 is reduced by 0.9 and 1.3 nm, respectively. Since the fully extended length of the DPP moiety is ca. 1.2 nm, this indicates that not all of the molecules are attaining a fully extended conformation normal to the surface in the cylindrical pore, which would reduce the mean pore diameter by ca. 2.4 nm.[18]

This conclusion is supported by preliminary molecular modeling and dynamics studies using the recently reported model of MCM-41 hexagonal mesoporous silica whose unit cell is derived from α-quartz.[19] Figure 5 shows a representative structure obtained from a 100-ps molecular dynamics (MD) simulation[19] at 375 °C for a MCM-41 silica (2.9 nm) containing grafted DPP molecules at a density of 1.33 DPP nm^{-2}, which is very similar to the maximum surface density of 1.37 DPP nm^{-2} that we measured experimentally for this pore size (Table 2, discussed in following section). As seen in Figure 5, the pore surface is well covered by DPP molecules, but not all of the molecules are fully extended into the pore interior. In any given frame of the MD simulation, or the energy-minimized structure, several DPP molecules are lying down on the silica pore surface. This is consistent with pore diameter measurements described above. Work is in progress to extend the model development to MCM-41 silicas with different pore sizes.

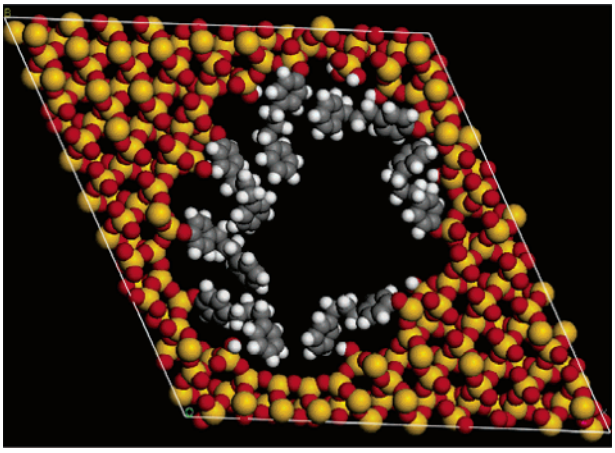

Figure 5. Model of MCM-41 silica (2.9-nm pore diameter) containing attached DPP molecules at a density of 1.33 nm^{-2}. Yellow, silicon; red, oxygen; gray, carbon; white, hydrogen.

Table 2. Surface Coverage Analysis for Organically Modified Silicas

silica	surface area[a] ($m^2\ g^{-1}$)	pore diameter[a] (nm)	$SiHMe_2$ coverage[b] (mmol g^{-1})	DPP coverage[c] (mmol g^{-1})	$SiHMe_2$ density[d] (nm^{-2})	DPP density[d] (nm^{-2})
Cabosil	200	n. a.	0.68	0.54	2.12	1.82
SBA-15	867	5.6	2.26	1.17	1.81	1.05
MCM-41	1088	2.9	2.97	1.67	1.99	1.37
MCM-41	1194	2.2	2.35	1.56	1.38	1.13
MCM-41	1285	1.7	1.92	1.46	1.00	0.96

[a] For the native silicas. [b] Surface coverage from carbon elemental analysis. [c] Average of the surface coverages obtained from chemical analysis (see text) and carbon elemental analysis (error is ±3%). [d] Molecular density of grafted groups (molecules/nm^2 surface area) corrected for the weight of the organic moiety.

Surface Coverage Dependence on Pore Size. Saturation surface coverages of DPP and $SiHMe_2$ were prepared on SBA-

(18) Derivatization of mesoporous silicas with alkylsilyl groups of varying chain lengths has been reported to give similar results in large pores, but a more extended conformation into the pores is detected for silicas with small pores that are slightly larger than the length of the alkylsilyl group. See: Antochshuk, V.; Kruk, M.; Jaroniec, M. *J. Phys. Chem. B* **2003**, *107*, 11900.

(19) Chaffee, A. L. *Fuel Process. Technol.*, published online Mar. 11, 2005 http://dx.doi.org/10.1016/j.fuproc.2005.01.013. MD studies made use of the Materials Studio suite of programs (Accelerys, Inc.), in particular the molecular simulation program DISCOVER and the COMPASS force field. COMPASS (Condensed-Phase Optimized Molecular Potentials for Atomistic Simulation Studies) has been parametrized by ab initio methods against a range of experimental observables for compounds incorporating H, C, N, O, S, P, Si, and halogens as well as others atoms. A mesoporous silica model with 3-D periodicity and a pore diameter of 2.9 nm was prepared starting from a 3-D infinite lattice of α-quartz. The internal surface of the mesopores was dehydrated using an iterative procedure (MD at progressively higher temperatures followed by dehydration of the most reactive H-bonded pairs of silanols) to provide a substrate with a surface hydroxyl concentration of 3.2 OH/nm^2, consistent with values expected for calcined silica surfaces. For the current work, the hydroxylated surface was functionalized with DPP at locations that provided the greatest energy relief calculated as the difference between the mean energies determined from MD runs of substrate and product (functionalized) structures. MD simulations were carried out for 100 ps at 375 °C, which corresponds to the temperature of the pyrolysis experiments. Typically, every 200th configuration was saved for analytical purposes.

15 and three MCM-41's of varying pore size (2.9, 2.2, and 1.7 nm), and the results were compared with a nonporous Cabosil fumed silica. The results are shown in Table 2, and repeat batch preparations gave the same results within ±5%. The $SiHMe_2$ surface coverages were obtained from carbon elemental analysis, while the DPP results are the average of the values obtained from elemental analysis and from chemical analysis following hydrolysis of DPP from the surface (see Experimental Section). The fact that the DPP results agree within ±3% provides confidence that the organic groups can be quantitatively recovered from the chemical analysis of the mesoporous silicas. In the last two columns of Table 2, the surface coverages are converted to surface densities (molecules nm^{-2}), which normalizes for the different surface areas of the silicas and different weights of the $SiHMe_2$ and DPP groups.

For comparison, our value for silylation of the 2.9 nm MCM-41 (1088 $m^2\ g^{-1}$) of 1.99 $SiHMe_2\ nm^{-2}$ agrees favorably with that obtained by Anwander for a related MCM-41 sample (2.8-nm pore diameter; 1139 $m^2\ g^{-1}$) of 1.85 $SiHMe_2\ nm^{-2}$.[6a] We observe that the silyl group densities are all smaller for the mesoporous silicas than those for the nonporous Cabosil, indicating a more crowded environment in the pores, and that the degree of silylation decreases with decreasing pore size (2.9−1.7 nm) for the structurally similar MCM-41 samples. Widenmeyer and Anwander recently observed similar behavior for silylation of the cubic phase MCM-48 over the pore size range of 3.8−1.6 nm and attributed the effect to increasing pore surface curvature at the smaller pore sizes resulting in increased steric crowding.[6b] It is interesting that silylation of the SBA-15 (5.6 nm) gives a $SiHMe_2$ density lower than that for the MCM-41 (2.9 nm) despite the large pore size. This result is a consequence of the significant amount of surface area in SBA-15 that is largely inaccessible in micropores (vide supra).

Derivatization of the silicas with the DPP groups follows the same trends as observed for the $SiHMe_2$ groups as shown in the last column of Table 2. However, the maximum degree of derivatization with DPP is consistently smaller than that for $SiHMe_2$, reflecting the larger size of the DPP group. We also note that, as in the silylation reaction, the density of DPP groups in the SBA-15 is smaller than that for the smaller pore MCM-41 (2.9 nm) sample, again reflecting the inaccessibility of the micropore surface area in SBA-15. However, it is clear that significant quantities of the DPP group can be grafted into the mesoporous silicas even at the small pore size of 1.7 nm, which is not significantly larger than the molecular length of 1.2 nm. This permits an investigation of the effect of pore confinement and pore size on chemical reaction kinetics and product compositions as described in a subsequent section.

NMR Investigations of Surface-Attached DPP. In recent NMR and transient fluorescence anisotropy measurements on aromatic molecules attached to the Cabosil silica surface, we found evidence for rapid rotational motion for these molecules at low surface densities.[20] In the current work, where DPP is confined in pores at high surface densities, we have examined the ^1H and ^{13}C NMR relaxation times for DPP to explore the potential impact of pore confinement and pore size on its motion. The effects, if present, might be particularly evident for the MCM-41 with the 1.7-nm pore diameter where DPP molecules (ca. 1.2 nm in length) have the potential to become intertwined. The $^1H-^{13}C$ CP/MAS ^{13}C NMR spectrum of DPP attached to the SBA-15 is shown in Figure 6. Similar spectra were observed for DPP on the other mesoporous silicas. The spin lattice relaxation times for these samples are given in Table 3 and are compared to those of the nonporous Cabosil.

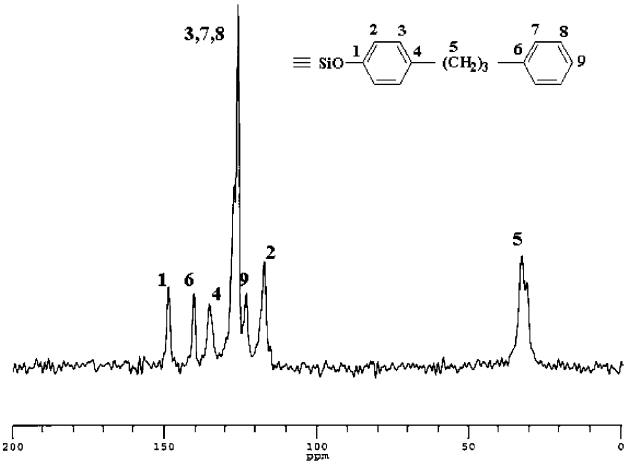

Figure 6. ^{13}C NMR spectrum of DPP attached to SBA-15.

Table 3. Spin Lattice Relaxation Times for Silica-Attached 1,3-Diphenylpropane[a]

silica[b]	$^1H\ T_1$ (s)	$^{13}C\ T_1$ (aromatic) (s)	$^{13}C\ T_1$ (aliphatic) (s)
Cabosil	0.34	0.22	0.13
SBA-15 (5.6 nm)	0.24	0.16	0.13
MCM-41 (2.0 nm)	0.28	0.22	0.17
MCM-41 (2.2 nm)	0.26	0.22	0.17
MCM-41 (1.7 nm)	0.22	0.16	0.15
average	*0.27 ± 0.05*	*0.20 ± 0.03*	*0.15 ± 0.02*

[a] Error is ±15−20%. [b] Pore diameter of native silica given in parentheses.

From NOE measurements on DPP attached to Cabosil at 100 °C, the NOE is near maximum ($\eta = 2.0$) for all protonated carbons in the sample. Hence, the dipole−dipole relaxation mechanism is the dominant relaxation pathway. From the near equivalence of the ^1H and ^{13}C T_1 values (Table 3), we conclude that the proton and carbon spin systems are efficiently coupled. The T_1 values are ca. 1 order of magnitude shorter than T_1's measured for neat 1,3-diphenylpropane, reflecting efficient coupling between the magnetic and lattice energies (i.e., a position on the T_1 versus τ_c (correlation time) near the minimum in the T_1 curve).[21] The difference between the aromatic and aliphatic ^{13}C T_1's is indicative of anisotropic motion. In the limit of isotropic motion the aromatic methine/aliphatic methylene ^{13}C T_1 ratio should be 2, the inverse of the ratio of the number of attached protons. The average value measured, 1.3, reflects the motional anisotropy of the diphenylpropane moiety due to its restricted reorientation motion, the consequence of its attachment to the silica surface. The ratio for diphenylpropane in solution is 1.8, revealing preferential rotation along the long axis of the molecule in solution.

The relaxation times in Table 3 show similar values, within experimental error, and are independent of pore size. The relaxation time measurements are most sensitive to motion

(20) Sigman, M. E.; Read, S.; Barbas, J. T.; Ivanov, I.; Hagaman, E. W.; Buchanan, A. C., III; Dabestani, R.; Kidder, M. K.; Britt, P. F. *J. Phys. Chem. A* **2003**, *107*, 3450.

(21) Slichter, C. P. In *Principles of Magnetic Resonance*, 2nd ed.; Springer-Verlag: Berlin, 1978; p 167.

Table 4. Pyrolysis Data for Surface-Attached 1,3-Diphenylpropane at 375 °C

silica	pore diameter[a] (nm)	DPP density (nm^{-2})	no. of pyrolyses	DPP conversion range (%)	rate[b] (% h^{-1})	correlation[c] (r^2)	selectivity[d] (styrene/toluene)
SBA-15	5.6	1.05	6	6.5−15.9	12.2	0.992	1.04
MCM-41	2.9	1.37	6	4.4−15.5	14.4	0.984	1.08
MCM-41	2.2	1.13	5	6.5−18.2	17.5	0.990	1.14
MCM-41	1.7	0.96	6	5.5−17.2	16.8	0.970	1.14

[a] For native silica. [b] Initial pyrolysis rate measured from the slope (linear regression) of a plot of percentage DPP conversion versus reaction time; typical error is ±5−10%. [c] Square of correlation coefficients for the regression analysis of the rate plots. [d] Initial reaction path selectivity measured from the styrene to toluene product yield ratios extrapolated to zero DPP conversion (see Figure 7).

Table 5. Comparison of DPP Rate Data for Mesoporous and Nonporous Silicas

silica[a]	DPP density (nm^{-2})	rate at 375 °C[b] (% h^{-1})
Cabosil	1.82	8.4
Cabosil	1.10	3.1[c]
Cabosil	0.43	0.39
Cabosil	0.31	0.26
SBA-15 (5.6 nm)	1.05	12.2
MCM-41 (2.9 nm)	1.37	14.4
MCM-41 (2.2 nm)	1.13	17.5
MCM-41 (1.7 nm)	0.96	16.8

[a] Cabosil data calculated from results of Buchanan et al.[8b,12] [b] Typical error in rates is ±5−10%. [c] Estimated from other Cabosil rate data; see text.

occurring at frequencies that are the inverse of the correlation time at the T_1 minimum, here ca. 10^9 rad s^{-1}. We conclude that any confinement effect imposed on the DPP moiety due to a change in its pore size environment is not associated with a significant change in reorientation motion in this frequency range.

Pore Confinement Effect on Pyrolysis Rate. Pyrolysis of the mesoporous silica-attached DPP samples at 375 °C produced gas-phase and surface-attached toluene and styrene (Scheme 1) as observed previously on the nonporous Cabosil surface.[8b,12] The initial reaction path selectivity, obtained from the relative yields of the gas-phase styrene and toluene, is given in Table 4 (last column) and will be discussed in the next section. Mass balances were quantitative within experimental error (±4%), indicating that all products were being retrieved from the porous solids. In one case, an SBA-15 (DPP) sample was examined after pyrolysis by nitrogen physisorption. The pore size distribution and mean pore diameter (4.7 nm) were identical to that for the sample prior to pyrolysis, indicating the ordered pore structure was being maintained during the pyrolysis experiments.

Initial reaction rates were measured from the slopes of the linear plots of DPP conversion versus reaction time with conversions limited to <20%, similar to the previous studies on Cabosil.[8b,12] The rates and correlation coefficients are given in Table 4, and repeat batches of DPP attached to SBA-15 and MCM-41 (2.9 nm) gave reproducible rates within ±5−10%. The reaction rates are compared in Table 5 with those previously reported for DPP on Cabosil,[8b,12] which were obtained at different DPP surface densities. The pyrolysis rates for DPP attached to the mesoporous silicas at saturation surface densities are all faster than those for DPP on Cabosil. To obtain a quantitative estimate of the effect of the pore confinement in enhancing the pyrolysis rate, the comparison must be made at similar DPP surface densities. The reason for this is shown in Table 5. The rates of the DPP reaction on Cabosil decrease dramatically with decreasing densities of DPP molecules on the surface, since the rates of the propagating hydrogen transfer steps, particularly on the surface, are greatly diminished. The approximate squared dependence of the rate on surface density can be used to estimate a rate for DPP on Cabosil at a density of ca. 1.10 nm^{-2}, which is the average DPP density for the mesoporous silica samples. The calculated rate on Cabosil is 3.1% h^{-1} [8.4% h^{-1}/(1.82 nm^{-2}/1.10 nm^{-2})^2]. Hence, the rate enhancement induced by pore confinement is a factor of 4 to 5 at 375 °C compared with the nonporous Cabosil at similar DPP surface densities.

This rate enhancement likely results from enhanced encounter frequencies within the pores for DPP molecules with chain carrying gas-phase and surface-attached benzyl radicals. In addition, the curved pore surface could lead to improved orientations for the hydrogen transfer between DPP molecules and the surface-attached benzyl radicals. This is supported by our recent demonstration that the rates of radical reactions on surfaces are sensitive to the orientation of molecular hydrogen donors co-attached to the surface.[8a,h] It is also interesting that the rates for the 1.7- and 2.2-nm MCM-41 samples are about 40% larger than that for the 5.6-nm SBA-15 sample at comparable surface densities of 1.0−1.1 nm^{-2}, suggesting that confinement in the smaller pores with the larger radius-of-curvature leads to faster rates.

Reaction Path Selectivity. Selectivity in product formation is determined by the relative rates of hydrogen abstraction at the two distinct benzylic methylene sites in surface-attached DPP, as shown in Scheme 1, since the rates of the subsequent β-scission steps for radicals **1** (≡$SiOPhCH{\cdot}CH_2CH_2Ph$) and **2** (≡$SiOPhCH_2CH_2CH{\cdot}Ph$) are comparatively fast. We have defined this regioselectivity, *S*, as the **2**:**1** ratio, which can be measured by the styrene/toluene gas-phase product ratio. Radical **1** is expected to be slightly more stable than radical **2** as a consequence of the stabilizing effect of the *para*-silyloxy surface linkage.[12] As a reference point, pyrolysis of *p*-$(CH_3)_3SiOPh(CH_2)_3Ph$ at 375 °C in fluid phases, in the absence of confinement effects, gave a value of $S = 0.91$, consistent with a small substituent effect for the *p*-silyloxy group favoring the formation of the analogue of **1**.[22]

The selectivity values for DPP on the mesoporous silicas are compared with those on Cabosil in Figure 7. The values of *S* increase with increasing DPP conversion for each material. The initial selectivities for the mesoporous silicas, obtained from the intercept values of linear regressions at zero DPP conversion, are listed in Table 4. Using the Cabosil case for reference, we note that this initial value of $S = 0.95$ is consistent with the anticipated small substituent effect of the silyloxy linkage favoring formation of **1**. The origin of the conversion dependence of the selectivity, which increasingly favors formation of the less thermodynamically stable radical, **2**, is not certain. However, as the reaction proceeds, increasing quantities of DPP molecules are converted into surface-bound product molecules, and subsequent hydrogen transfers may have to occur over

(22) The related *p*-methoxy group has also been reported to be a mildly stabilizing substituent for benzyl radicals. Creary, X. *J. Org. Chem.* **1980**, *45*, 280.

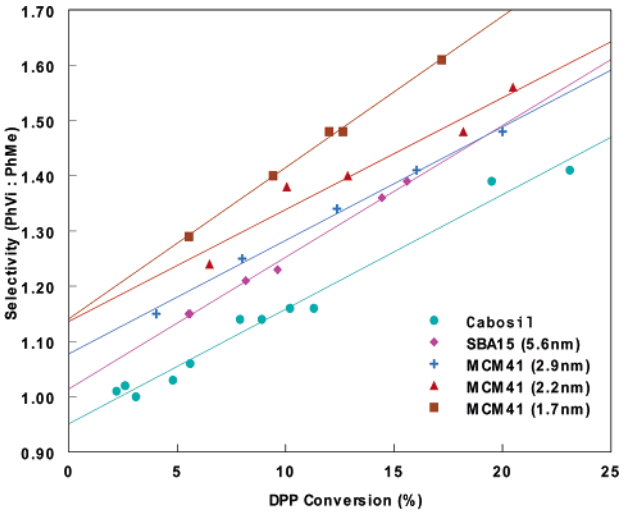

Figure 7. Regioselectivity in the pyrolysis of DPP as a function of the support monitored by the ration of yields of gas-phase styrene to toluene.

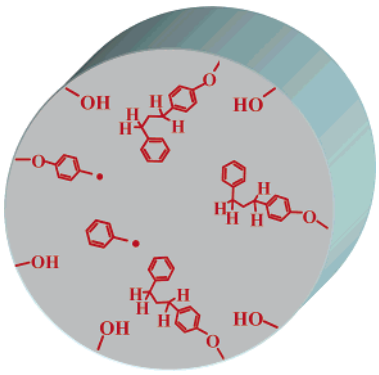

Figure 8. Illustration of potential regioselectivity in hydrogen abstraction by gas-phase and surface-attached benzyl radicals based on accessibility of the DPP benzylic methylene sites in the pores.

longer distances and in the presence of these intervening product molecules. This may lead to an increasing preference for hydrogen abstraction at the benzylic methylene site farthest from the surface, which could be more accessible.

The selectivities for DPP on the mesoporous silicas show a similar dependence on DPP conversion (Figure 7). However, it is clear that as the pore size decreases, the values for *S* increase when compared at similar DPP conversion. In addition, the *S* values are all greater that 1.0 even when extrapolated to zero conversion. Hence, hydrogen abstraction in the porous solids slightly favors the formation of the least stable radical, **2**, and this becomes increasingly important as the pore size decreases (and the pore wall radius-of-curvature increases). Clearly this must be a consequence of accessibility of the DPP benzylic methylene hydrogens to the chain carrying benzylic radicals as illustrated in Figure 8. The benzylic methylene hydrogens farthest from the surface must be more accessible to the gas-phase and nearby surface-attached benzyl radicals, and it is anticipated that the largest impact would be on the hydrogen transfer to the surface-confined benzyl radical. This hypothesis must be tested in more rigorous and realistic models such as the one shown in Figure 5. Molecular dynamics simulations on these model mesoporous silica surfaces as a function of pore size are in progress, which should provide additional insights into the origins of the impact of pore confinement and size on the hydrogen transfer selectivity. The consequence of the pore confinement effects is a substantial alteration of the regioselectivity for product formation in the mesoporous solids compared with homogeneous phases. For example, confinement in the 1.7-nm pore size MCM-41 results in a selectivity value of ca. 1.6 at only 15% DPP conversion compared with the value of 0.91 for the solution-phase analogue (vide supra). This suggests that pore confinement effects in mesoporous solids can be used to control chemical reactivity and alter product selectivities compared with solution-phase behavior.

Conclusions

These studies have shown a new method for derivatization of mesoporous silicas with aromatic phenols to give hybrid materials possessing silyl aryl ether linkages to the surface. This type of linkage has the advantages of being thermally stable to high temperature and being easily hydrolyzed with aqueous base to quantitatively recover the organics. This allows facile product analysis following a reaction such as thermolysis, photolysis, and so forth. The method was demonstrated for mesoporous silicas with a range of pore sizes (5.6−1.7 nm), and significant quantities of long (ca. 1.2 nm), flexible DPP molecules could be grafted even into a 1.7-nm pore diameter MCM-41 silica. As anticipated, the maximum density of surface-attached molecules decreased with decreasing pore size as a consequence of steric crowding. This method should be readily extended to other phenolic structures, as well as to alcohols, which we are continuing to investigate.

Pore confinement effects were examined in the free-radical chain pyrolysis of DPP and compared with the nonporous Cabosil silica. Pore confinement was shown to lead to significant increases in the pyrolysis rate, and the rates increased modestly with decreasing pore size. This effect is attributed to enhanced encounter frequencies in the pores that accelerate the key hydrogen transfer steps, as well as to improved orientations for the hydrogen transfers on the surface. Pore confinement also results in alterations in the regioselectivity of the thermolysis reaction by favoring hydrogen abstractions from the thermodynamically less favored, but more accessible, benzylic methylene in DPP that is farthest from the surface. This effect is also magnified in the smaller pore sizes where the pore radius-of-curvature increases. These studies have shown that pore confinement can alter chemical reactivity in mesoporous solids, and control of these effects could be important in areas ranging from catalysis to the synthesis of novel materials.

Acknowledgment. This research was sponsored by the Division of Chemical Sciences, Geosciences, and Biosciences, Office of Basic Energy Sciences, U.S. Department of Energy under Contract DE-AC05-00OR22725 with Oak Ridge National Laboratory, managed and operated by UT-Battelle, LLC. We also acknowledge Mr. Avi Waksburg for skilled technical support in the molecular modeling and dynamics studies.

JA050389W